

Rock-salt SnS and SnSe: Native Topological Crystalline Insulators

Yan Sun^{1,2,3}, Zhicheng Zhong⁴, Tomonori Shirakawa^{2,5,6}, Cesare Franchini³,
Dianzhong Li¹, Yiyi Li¹, Seiji Yunoki^{2,5,6,7}, and Xing-Qiu Chen^{1*}

¹ *Shenyang National Laboratory for Materials Science, Institute of Metal Research,
Chinese Academy of Sciences, Shenyang 110016, China,*

² *Computational Condensed Matter Physics Laboratory, RIKEN, Wako, Saitama 351-0198, Japan,*

³ *Computational Materials Physics, Faculty of Physics,
University of Vienna, Sensengasse 8/7, A-1090 Vienna, Austria,*

⁴ *Institute of Solid State Physics, Vienna University of Technology, 1040 Vienna, Austria,*

⁵ *CREST, Japan Science and Technology Agency (JST), Kawaguchi, Saitama 332-0012, Japan,*

⁶ *Computational Materials Science Research Team,
RIKEN Advanced Institute for Computational Science (AICS), Kobe, Hyogo 650-0047, Japan, and*

⁷ *Computational Quantum Matter Research Team,*

RIKEN Center for Emergent Matter Science (CEMS), Wako, Saitama 351-0198, Japan

(Dated: June 21, 2018)

Unlike time-reversal topological insulators, surface metallic states with Dirac cone dispersion in the recently discovered topological crystalline insulators (TCIs) are protected by crystal symmetry. To date, TCI behaviors have been observed in SnTe and the related alloys $\text{Pb}_{1-x}\text{Sn}_x\text{Se/Te}$, which incorporate heavy elements with large spin-orbit coupling (SOC). Here, by combining first-principles and *ab initio* tight-binding calculations, we report the formation of a TCI in the relatively lighter rock-salt SnS and SnSe. This TCI is characterized by an even number of Dirac cones at the high-symmetry (001), (110) and (111) surfaces, which are protected by the reflection symmetry with respect to the $(\bar{1}10)$ mirror plane. We find that both SnS and SnSe have an intrinsically inverted band structure and the SOC is necessary only to open the bulk band gap. The bulk band gap evolution upon volume expansion reveals a topological transition from an ambient pressure TCI to a topologically trivial insulator. Our results indicate that the SOC alone is not sufficient to drive the topological transition.

PACS numbers: 73.20.At, 71.20.-b, 71.70.Ej

Since the discovery of Z_2 topological insulators (TIs) [1, 2], band topological properties in condensed matter physics have attracted increasing interest as a new physical paradigm, which also shows great promise for potentially revolutionary applications in quantum computing and spintronics. TIs possess a non-trivial time-reversal Z_2 topological invariant and the topological characteristics are manifested by the presence of an odd number of linearly dispersing Dirac cones at the crystal surfaces. These surface metallic states are due to large spin-orbit coupling (SOC) and are protected by time-reversal symmetry [1, 2].

In 2011, Liang Fu proposed a theoretical model for an alternative class of topological states, named topological crystalline insulators (TCIs), in which the gapless surface states are protected not by time-reversal symmetry but by crystal symmetry [3, 4]. Up to now, the only reported TCIs are the narrow band gap semiconductor SnTe and the related alloys $\text{Pb}_{1-x}\text{Sn}_x\text{Se/Te}$ [5–9]. Very recently, Barone *et al.* have theoretically predicted that a suitable combination of applied pressure and alloying can turn rock-salt lead chalcogenides, such as PbSe, PbTe, and PbS, into TCIs [10]. The most prominent feature of this class of TCIs is the presence of an even, not odd as in TIs, number of Dirac cones which lay on surface terminations oriented perpendicular to the mirror symmetry planes. It is shown that the necessary conditions

for the band inversions to occur in all these TCIs are (i) a strongly asymmetric hybridization between cation (anion) s and anion (cation) p states and (ii) a sizable SOC strength, similarly in time-reversal TIs [11–18]. Large SOC is recognized to be a crucial ingredient to form possible TCIs also in pyrochlore oxides $A_2\text{Ir}_2\text{O}_7$, where A is a rare-earth element [19]. However, TCIs can be considered as the counterpart of TIs in materials without SOC [3]. Thus, it is of fundamental importance to seek a manifestation of the non-trivial crystalline topology in materials composed of constituents with lighter mass and thus smaller SOC, for which the SOC effect is detached from the formation of TCIs.

In this Letter, through first-principles calculations along with Wannier functions based *ab initio* tight-binding (TB) modeling, we report that rock-salt SnS and SnSe are both TCIs in their native phase without any alloying or applied strain/pressure. We find that their inverted band order is induced by chemical bonding and crystal field, whereas the SOC effect is only to open the bulk band gap. This non-trivial topological state is substantiated by the emergence of an even number of Dirac cones at the high-symmetry crystal surfaces perpendicular to the $(\bar{1}10)$ mirror symmetry plane. We also demonstrate that a topological transition occurs to a trivial insulator upon volume expansion.

First-principles calculations based on density func-

tional theory (DFT) are performed in the generalized gradient approximation (GGA), following the Perdew-Burke-Ernzerhof parametrization scheme [20], with the projected augmented wave method as implemented in the Vienna *Ab initio* Simulation Package (VASP) [21, 22]. The energy cutoff is set to be 500 eV. The TB matrix elements are calculated by projection onto maximally localized Wannier orbitals [23–25], using the VASP2WANNIER90 interface [26].

Early experimental characterizations [27–29] have found that both SnS and SnSe crystallize in low temperatures *Pnma* GeS-type orthorhombic phase [30] and that at high temperatures two metastable orthorhombic *Cmcm* TII-type [30] and rock-salt cubic NaCl-type phases [29] (Fig. 1) exist. Here, we focus on the rock-salt structure, which has been shown to be stable under epitaxial growth of SnSe and SnS on a NaCl substrate with lattice constants $a_{\text{Expt}}^{\text{SnSe}} = 5.99 \text{ \AA}$ [28] and $a_{\text{Expt}}^{\text{SnS}} = 6.00 \text{ \AA}$ [28] and 5.80 \AA [31], respectively. Our first-principles calculations find that the optimized lattice constants are $a_{\text{Theo}}^{\text{SnSe}} = 6.05 \text{ \AA}$ and $a_{\text{Theo}}^{\text{SnS}} = 5.85 \text{ \AA}$ for SnSe and SnS, respectively, in good agreement with the experimental values.

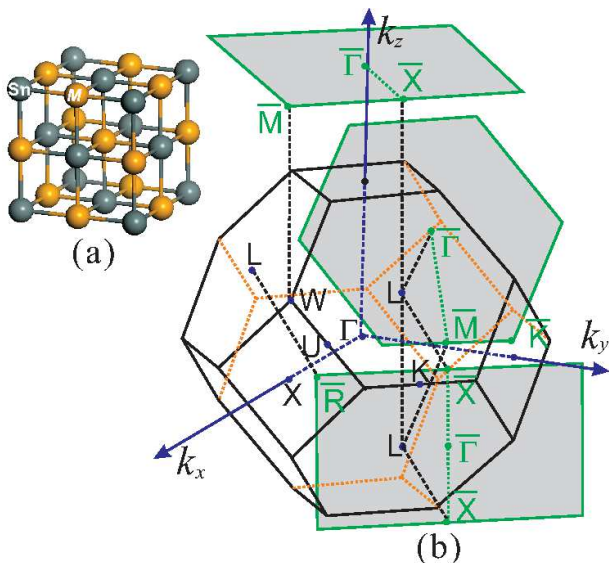


FIG. 1: (color online) (a) $\text{Sn}M$ ($M = \text{S}$ and Se) rock-salt lattice structure and (b) face cubic centered (FCC) Brillouin zone (BZ). Two dimensional BZ projected onto the (001), (110), and (111) surfaces are also shown in (b). These three surfaces are all perpendicular to the $(\bar{1}10)$ mirror symmetry plane.

Bulk band structure. The calculated bulk band structures along the high symmetry lines around L in the Brillouin zone (BZ) are shown in Fig. 2 (a)–(d), and for comparison the results for those of the isostructural TCI SnTe are also plotted in Fig. 2 (e) and (f) [5, 7]. The band structures of SnS, SnSe, and SnTe display similar

features, which are summarized as follows: (i) Without SOC, all compounds have a gapless three dimensional (3D) Dirac cone located in the vicinity of the high symmetry L point along the L - W line; (ii) Level anticrossing occurs once SOC is included and the 3D Dirac cone is broken with opening a finite band gap; (iii) The top of the valence band and the bottom of the conduction band at and near L are primarily composed of Sn p -like and S/Se/Te p -like states, respectively; (iv) The parity of the top (bottom) of the valence (conduction) band at L is odd (even); (v) The band character around L remains unchanged upon including SOC. These features already indicate that rock-salt SnS and SnSe are TCIs just like SnTe [34]. It should be emphasized here that, unlike TIs [11–18], the inverted band order is found to be driven not by SOC but solely by chemical bonding and crystal field [see Fig. 2 (j)].

The occurrence of band inversion at an even number of \mathbf{k} points (i.e., four equivalent L points) and the fact that this band inversion is not driven by SOC are suggestive of the formation of a crystal-symmetry driven non-trivial topological state. In order to provide further support, let us study the evolution of the band gap as a function of the lattice constant. It is an obvious fact that any insulator is topologically trivial in the atomic limit. Therefore, the occurrence of inverted band order implies that the band gap has to close and re-open by progressively increasing the lattice constant. This behavior is indeed found in Fig. 2 (i): The band gap E_g at L closes with increasing the lattice constant and then re-opens with the opposite band character, i.e., the parity as well as the main contributing weight of the constituent atoms being reversed for the top of the valence band and the bottom of the conduction band [Fig. 2 (d) and (h)]. These results clearly demonstrate that a topological phase transition from a topologically non-trivial to a trivial states occurs with increasing the lattice constant. Note that a similar behavior is found even without including SOC [Fig. 2(c) and (g)], indicating that SOC has indeed no influence in determining the band character around L . The evolution of the band character is schematically drawn in Fig. 2 (j).

To quantify the topological feature, we shall evaluate the mirror Chern number. We first calculate the Berry curvature $\Omega^m(\mathbf{k}) = \nabla_{\mathbf{k}} \times \mathbf{A}^m(\mathbf{k})$ on the $(\bar{1}10)$ mirror symmetry plane in the BZ. Here, $\mathbf{A}^m(\mathbf{k}) = i \sum_n \langle u_n^m(\mathbf{k}) | \nabla_{\mathbf{k}} | u_n^m(\mathbf{k}) \rangle$ is the Berry connection, $u_n^m(\mathbf{k})$ is the n -th eigenstate at momentum \mathbf{k} and with mirror eigenvalue $m (= \pm i)$ of the TB model described below, and the sum is over all occupied bands. The results of the component $\Omega_{\perp}^m(\mathbf{k})$ perpendicular to the $(\bar{1}10)$ mirror plane are shown in Fig. 3 for SnSe with both experimental and expanded lattice constants. We find that the main contributions are from momenta close to L and that $\Omega_{\perp}^{+i}(\mathbf{k}) = -\Omega_{\perp}^{-i}(\mathbf{k})$. We evaluate the mirror Chern number [35], $c_M = (n_{+i} - n_{-i})/2$, where $n_m = \int \Omega^m(\mathbf{k}) \cdot d\mathbf{S}$, and find that $c_M = -2(0)$ for SnSe with the experi-

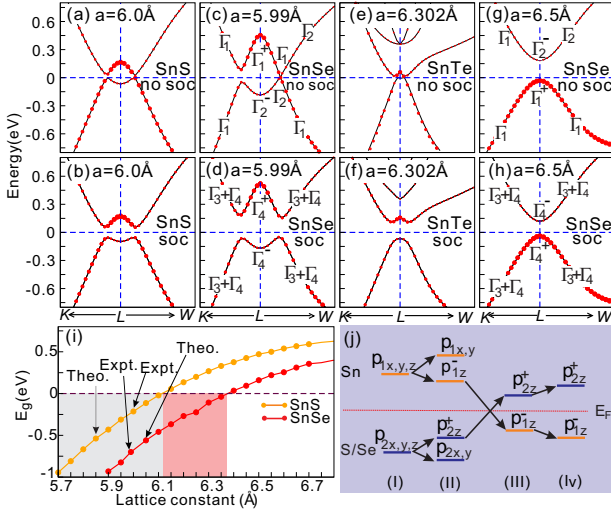


FIG. 2: (color online) (a-h): Electronic band structures obtained by first-principles calculations for SnS (a,b), SnSe (c,d,g,h), and SnTe (e,f) with and without SOC. The size of red dots in (a)-(h) is proportional to the amount of contributing weight in each band from S (a,b), Se (c,d,g,h), or Te (e,f) atoms. In (a)-(f), the experimental lattice constant a (indicated in the figures) is used [32], whereas in (g) and (h) an expanded lattice constant is used. The irreducible representations of the bands closest to Fermi energy (set to be 0) are also indicated [33]. (i): The evolution of the band gap E_g calculated with SOC as a function of the lattice constants for SnS and SnSe. The energy gap E_g is defined as the energy difference between the top of the valence band and the bottom of the conduction band at L , i.e., $E_g = E_-^L - E_+^L$, where E_p^L is the band energy with parity p ($= +, -$) at L . Thus, E_g is negative when the bands are inverted order. The optimized and experimental lattice constants are indicated by arrows, all located within the non-trivial topological region. (j) A schematic energy level diagram around L : (I) atomic limit, (II) including hybridization with a large lattice constant, (III) with the experimental lattice constant, and (IV) inclusion of SOC. The band is inverted already in (III) without SOC. Here E_F stands for Fermi energy. The signs ($+, -$) denote the parities of the corresponding p -like orbitals.

mental (expanded) lattice constant, confirming the topological transition from a TCI to a trivial insulator with increasing the lattice constant. We also calculate the Z_2 indices ($\nu_0; \nu_1\nu_2\nu_3$) [36] and find that this index is (0; 000) [see Fig. 3 (c)] for SnSe with both experimental and expanded lattice constants, suggesting that they are not time-reversal Z_2 TIs.

Surface band structure. Let us next examine the intrinsic properties of the topological phase in SnS and SnSe, and provide further evidence of this TCI state by inspecting the surface properties. Unlike TIs for which an odd number of Dirac cones appears in any surface orientation, TCIs have an even number of topologically protected Dirac cones on high symmetry surfaces. For the rock-salt crystal structure, gapless surface states are

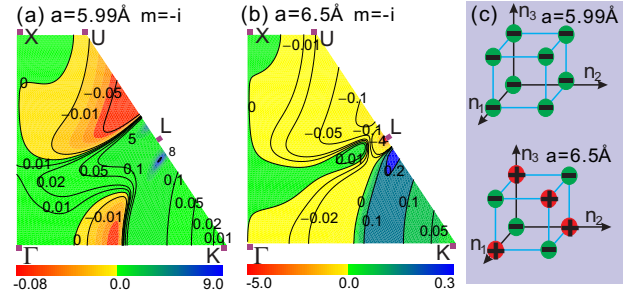


FIG. 3: (color online) Contour plots of the Berry curvature $\Omega^m(\mathbf{k})$ on the $(\bar{1}10)$ mirror symmetry plane in the BZ for SnSe with the experimental lattice constant $a=5.99\text{\AA}$ (a) and with an expanded lattice constant $a=6.5\text{\AA}$ (b). Only the component $\Omega_{\perp}^m(\mathbf{k})$ perpendicular to the $(\bar{1}10)$ mirror plane with $m = -i$ is plotted. Note that $\Omega_{\perp}^{+i}(\mathbf{k}) = -\Omega_{\perp}^{-i}(\mathbf{k})$. The high symmetry momenta, $\mathbf{k} = n_1\mathbf{b}_1/2 + n_2\mathbf{b}_2/2 + n_3\mathbf{b}_3/2$, are indicated in (a) and (b) by $\Gamma : (n_1, n_2, n_3) = (0, 0, 0)$, $X : (1, 1, 0)$, $U : (\frac{5}{4}, \frac{5}{4}, \frac{1}{2})$, $L : (1, 1, 1)$, and $K : (\frac{3}{4}, \frac{3}{4}, \frac{3}{2})$ with the reciprocal lattice vectors $\mathbf{b}_1 = \frac{2\pi}{a}(-1, 1, 1)$, $\mathbf{b}_2 = \frac{2\pi}{a}(1, -1, 1)$, and $\mathbf{b}_3 = \frac{2\pi}{a}(1, 1, -1)$. (c) The products of parity eigenvalues from the occupied states ($\delta_{n_1 n_2 n_3} = \pm 1$) at eight time reversal momenta \mathbf{k} , i.e., $n_1, n_2, n_3 = 0, 1$, are indicated for SnSe with both experimental and expanded lattice constants.

expected to exist only on surfaces which are perpendicular to the $(\bar{1}10)$ mirror symmetry planes [5, 9, 37].

To prove these expectations, we shall now compute the band dispersions for the (001), (110) and (111) surfaces [see Fig. 1 (b)] using the *ab initio* TB model. The *ab initio* TB model is constructed by downfolding the bulk energy bands, obtained by first-principles calculations, using maximally-localized Wannier functions (MLWFs). As the bulk energy bands near Fermi energy are predominantly formed by hybridized p -like Sn and S/Se orbitals, the MLWFs are derived from atomic p -like orbitals and the TB parameters are determined from the MLWFs overlap matrix. The SOC is considered here in the atomic form:

$$H_{\text{SO}}^p(\lambda) = \frac{\lambda}{2} \begin{bmatrix} 0 & 0 & -i & 0 & 0 & 1 \\ 0 & 0 & 0 & i & -1 & 0 \\ i & 0 & 0 & 0 & 0 & -i \\ 0 & -i & 0 & 0 & -i & 0 \\ 0 & -1 & 0 & i & 0 & 0 \\ 1 & 0 & i & 0 & 0 & 0 \end{bmatrix} \quad (1)$$

with p -like orbital bases $\{|p_x, \uparrow\rangle, |p_x, \downarrow\rangle, |p_y, \uparrow\rangle, |p_y, \downarrow\rangle, |p_z, \uparrow\rangle, |p_z, \downarrow\rangle\}$, where arrows indicate electron spins. The SOC parameter λ for Sn, Se, and S are taken from experimental spectral data, i.e., $\lambda_{\text{Sn}}=0.27\text{ eV}$, $\lambda_{\text{Se}}=0.22\text{ eV}$, and $\lambda_{\text{S}}=0.05\text{ eV}$, respectively [38]. The quality of the TB parametrization is successfully assessed in Fig. 4, where the TB bulk band structures are compared with the corresponding first-principles results.

Encouraged by this quantitative agreement, let us finally compute the surface band structures by adopting

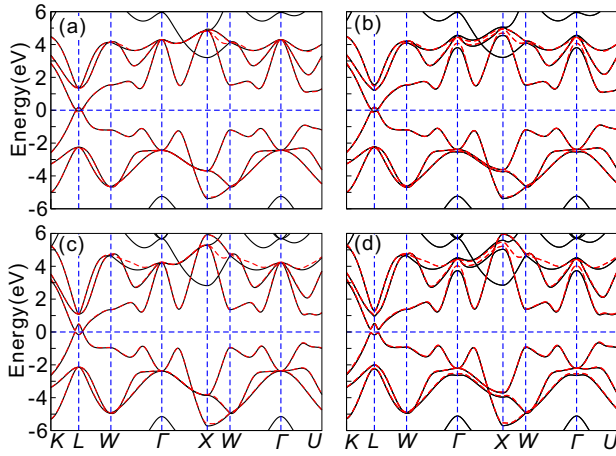


FIG. 4: (color online) Comparison of the bulk energy band structures obtained from the *ab initio* TB model (red dashed lines) and from the first-principles calculations (black solid lines) for rock-salt SnS (a,b) and SnSe (c,d). Figures (a,c) and (b,d) correspond to the cases without and with including SOC, respectively.

three slabs for the (001), (110), and (111) surfaces with thickness of 89, 89, and 239 atomic layers, respectively. The results of the TB calculations are summarized in Fig. 5. These results show clearly that the (001), (110), and (111) surfaces with the experimental lattice constants possess metallic states with opposite mirror eigenvalues which cross each other forming a massless Dirac cone. It has been shown [5, 9] that the rock-salt TCIs with the mirror Chern number $c_M = -2$ guarantees the presence of two pairs of counter-propagating, spin-resolved surface states with opposite mirror eigenvalues along all symmetrically equivalent $\bar{\Gamma}$ - \bar{X} lines in the (100) surface, and only one pair in the (110) surface [Fig. 1 (b)]. Indeed, both SnS and SnSe surfaces follow this symmetry consideration, displaying four equivalent Dirac cones in the (001) surface [Fig. 5 (a) and (e)] and two Dirac cones in the (110) surface [Fig. 5 (b) and (f)]. Instead, similarly to the case of SnTe [9], four Dirac cones are found in the (111) surface, one at $\bar{\Gamma}$ and other three at \bar{M} , as shown in Fig. 5 (c), (d), (g), and (h).

In addition, as already shown in Fig. 2 (i) and Fig. 3, for the lattice constants larger than 6.10 Å for SnS and 6.37 Å for SnSe, the band character changes and the systems undergo a topological transition towards a trivial insulator. This is clearly reflected also in the surface band structures computed for SnSe with the lattice constant $a = 6.50$ Å in Fig. 5 (i)-(l): the Dirac cones disappear and a broad spectral feature develops on the top (bottom) of the valence (conduction) band with a finite band gap, a typical behavior of an ordinary trivial insulator. These results unambiguously demonstrate that rock-salt SnSe and SnS represent the features of TCI.

In conclusion, using first-principles calculations to-

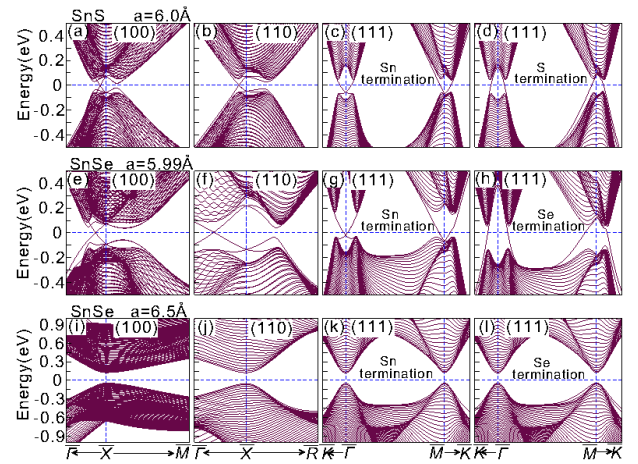


FIG. 5: (color online) TB energy band structures of the (100), (110), and (111) surfaces for rock-salt (a-d) SnS with the experimental lattice constant $a=6.0$ Å, (e-h) SnSe with the experimental lattice constant $a=5.99$ Å, and (i-l) SnSe with an expanded lattice constant $a=6.5$ Å. Notice that there exist two distinct surface terminations for the (111) surface. In (a)-(h) the appearance of the gapless Dirac-cone-like metallic states evidences the occurrence of TCI. With expanding the lattice constant in (i)-(l), Dirac-cone-like metallic surface states disappear, suggesting that the system is a trivial insulator. The surface projected momenta are indicated in Fig. 1(b).

gether with *ab initio* tight-binding model analyses, we have revealed that rock-salt SnS and SnSe represent a prime example of topological crystalline insulators at ambient pressure without incorporating heavy elements. We have shown that in both systems an even number of symmetry-protected Dirac cones emerge in the (100), (110), and (111) surfaces perpendicular to the $(\bar{1}10)$ mirror symmetry plane. We have also shown that the spin-orbit coupling is still important to open the band gap in the bulk phases although it is not necessary to drive the topologically non-trivial state with the inverted band order, as proposed in the original theory [3]. We have also demonstrated that a topological transition occurs toward a trivial insulator upon volume expansion. Finally, we emphasize that the onset of the topological crystalline insulating state in SnS and SnSe is not dependent on alloying, strain, pressure, or any electronic structure engineering, but SnS and SnSe are both topological crystalline insulators in their native phase.

This work was supported by the ‘‘Hundred Talents Project’’ of the Chinese Academy of Sciences, NSFC of China (grant numbers 51074151 and 51174188), and Grant-in-Aid for Scientific Research from MEXT Japan (grant numbers 24740269 and 25287096). We acknowledge Vienna Scientific Cluster, Beijing Supercomputing Center of CAS (including in Shenyang branch), and RIKEN Cluster of Clusters (RICC) facility for computa-

tional resources.

* Corresponding author: xingqiu.chen@imr.ac.cn

- [1] M. Z. Hasan and C. L. Kane, *Rev. Mod. Phys.* **82**, 3045 (2010).
- [2] X. L. Qi and S. C. Zhang, *Rev. Mod. Phys.* **83**, 1057 (2011).
- [3] L. Fu, *Phys. Rev. Lett.* **106**, 106802 (2011).
- [4] Also see R.-J. Slager, A. Mesaros, V. Juričić, and J. Zaanen, *Nature Phys.* **9**, 98 (2013).
- [5] T. H. Hsieh, H. Lin, J. Liu, W. Duan, A. Bansil, and L. Fu, *Nature Comms.* **3**, 982 (2012).
- [6] P. Dziawa, B. J. Kowalski, K. Dybko, R. Buczko, A. Szczerbakow, M. Szot, E. Lusakowska, T. Balasubramanian, B. M. Wojek, M. H. Berntsen, O. Tjernberg, T. Story P. Dziawa, B. J. Kowalski, K. Dybko, R. Buczko, A. Szczerbakow, M. Szot, E. Lusakowska, T. Balasubramanian, B. M. Wojek, M. H. Berntsen, O. Tjernberg, and T. Story, *Nature Mater.* **11**, 1023 (2012).
- [7] Y. Tanaka, Z. Ren, T. Sato, K. Nakayama, S. Souma, T. Takahashi, K. Segawa, and Y. Ando, *Nature Phys.* **8**, 800 (2012).
- [8] S. Y. Xu, C. Liu, N. Alidoust, D. Qian, M. Neupane, J. D. Denlinger, Y. J. Wang, H. Lin, L. A. Wray, R. J. Cava, A. Marcinkova, E. Morosan, A. Bansil, and M. Z. Hasan, *Nature Comms.* **3**, 1192, (2012).
- [9] J. Liu, W. Duan, and L. Fu, arXiv:1304.0430.
- [10] P. Barone, T. Rauch, D. D. Sante, J. Henk, I. Mertig, and S. Picozzi, *Phys. Rev. B* **88**, 045207 (2013); P. Barone, D. D. Sante, and S. Picozzi, arXiv:1308.1288.
- [11] Y. Xia, D. Qian, D. Hsieh, L. Wray, A. Pal, H. Lin, A. Bansil, D. Grauer, Y. S. Hor, R. J. Cava, and M. Z. Hasan, *Nature Phys.* **5**, 398 (2009).
- [12] H. Zhang et al., *Nature Phys.* **5**, 438 (2009); C. X. Liu, X. L. Qi, H. Zhang, X. Dai, Z. Fang, and S. C. Zhang, *Phys. Rev. B* **82**, 045122 (2010).
- [13] H. Z. Lu, W. Y. Shan, W. Yao, Q. Niu, and S. Q. Shen, *Phys. Rev. B* **81**, 115407 (2010).
- [14] J. G. Analytis, J. H. Chu, Y. Chen, F. Corredor, R. D. McDonald, Z. X. Shen, and I. R. Fisher, *Phys. Rev. B* **81**, 205407 (2010).
- [15] D. Xiao, Y. Yao, W. Feng, J. Wen, W. Zhu, X.-Q. Chen, G. M. Stocks, and Z. Zhang, *Phys. Rev. Lett.* **105**, 096404 (2010).
- [16] Y. Sun, X.-Q. Chen, S. Yunoki, D. Li, and Y. Li, *Phys. Rev. Lett.* **105**, 216406 (2010).
- [17] Y. Sun, X.-Q. Chen, C. Franchini, D. Li, S. Yunoki, Y. Li, and Z. Fang, *Phys. Rev. B* **84**, 165127 (2011).
- [18] Y. Chen, *Front. Phys.* **7**, 175 (2012).
- [19] M. Kargarian and G. A. Fiete, *Phys. Rev. Lett.* **110**, 156403 (2013).
- [20] J. P. Perdew, K. Burke, and M. Ernzerho, *Phys. Rev. Lett.* **77**, 3865 (1996).
- [21] G. Kresse and J. Hafner, *Phys. Rev. B* **48**, 13115, (1993).
- [22] G. Kresse and J. Furthmüller, *Comp. Mater. Sci.* **6**, 15 (1996).
- [23] N. Marzari and D. Vanderbilt, *Phys. Rev. B* **56**, 12847 (1997).
- [24] I. Souza, N. Marzari, and D. Vanderbilt, *Phys. Rev. B* **65**, 035109 (2001).
- [25] A. A. Mostofi, J. R. Yates, Y. S. Lee, I. Souza, D. Vanderbilt, and N. Marzari, *Comput. Phys. Commun.* **178**, 685 (2008).
- [26] C. Franchini, R. Kovik, M. Marsman, S. S. Murthy, J. He, C. Ederer, and G. Kresse, *J. Phys.: Condens. Matter* **24**, 235602 (2012).
- [27] P. M. Nikolic, *Brit. J. Appl. Phys.* **16**, 1075 (1965).
- [28] A. N. Mariano and K. L. Chopra, *Appl. Phys. Lett.* **10**, 282 (1967).
- [29] L. S. Palatnik and V. V. Levitin, *Doklady Akademii Nauk SSSR* **96**, 975-978 (1995).
- [30] T. Chattopadhyay, J. Pannetier, and H. G. Von Schnering, *J. Phys. Chem. of Solids* **47**, 879 (1986).
- [31] B. F. Bilenkii, A. G. Mikolaichuk, and D. M. Freik, *Phys. Status Solidi* **28**, K5 (1968).
- [32] For the lattice constant of SnTe, see R. Marx and K. J. Range, *J. Less-Common Met.* **155**, 49 (1989).
- [33] Although not shown for clarity, the same irreducible representations are assigned to the bands of SnS and SnTe. Note that the origin of the symmetry operations is set to Sn atom.
- [34] One of the important quantitative differences is that the band gap E_g of SnSe ($E_g \sim 0.202$ eV) seems larger than SnTe ($E_g \sim 0.172$ eV). However, more careful study beyond GGA is required for better quantitative comparison.
- [35] J. C. Y. Teo, L. Fu, and C. L. Kane, *Phys. Rev. B* **78**, 045426 (2008).
- [36] L. Fu, C. L. Kane, and E. J. Mele, *Phys. Rev. Lett.* **98**, 106803 (2007).
- [37] S. Safaei, P. Kacman, and R. Buczko, *Phys. Rev. B* **88**, 045305 (2013).
- [38] K. Wittel and R. Manne, *Theor. Chim. Acta* **33**, 347 (1974).